

## Theoretical Study on the Mechanism of the NCO + HCNO Reaction

Bu-Tong Li,<sup>\*,†</sup> Jian Zhang,<sup>†</sup> Hai-Shun Wu,<sup>†</sup> and Guang-Dong Sun<sup>‡</sup>*Department of Chemistry, Shanxi Normal University, Linfen, Shanxi, 041004, China, and Department of Nephropathy, Second Hospital of Jilin University, Changchun, Jilin, 130041, China**Received: April 4, 2007; In Final Form: May 26, 2007*

The complex doublet potential surface of the NCO + HCNO reaction has been investigated at the QCISD-(T)/6-311g(d,p)//UB3LYP/6-31G(d,p) level. We have found 29 isomers on the potential surface, which are connected by 38 transition states. The single-point energy calculations are performed at the high-level QCISD-(T)/6-311G(d,p) for more accurate energy values. In various possible initial association ways, the end-N attack leading to HC<sub>2</sub>N<sub>2</sub>O<sub>2</sub> **a1** and **a2** is the most favorable association way through a barrierless process. Through the thermodynamic and kinetic analyses, the product NO + CO + HCN should be the major product in both the low- and high-temperature conditions for its low-energy determination transition state. Our calculation is consistent with the available data in low-temperature condition and expected to be confirmed in the high-temperature condition.

## Introduction

The fate of the HCNO molecule, as the important intermediate molecule in the NO-reburning process for the reduction of NO<sub>x</sub> pollutants, has been an interesting aspect for the atmosphere chemistry and the combustion chemistry.<sup>1</sup> NCO is also an important intermediate in several combustion environments, including the PAPRENO<sub>x</sub> process for reducing NO<sub>x</sub> emissions.<sup>2–4</sup> Thermodynamic information on the reactants and products are available,<sup>5–8</sup> but only one kinetic study has been reported, with the major product channel identified as NO + CO + HCN, and a total rate constant of  $(1.58 \pm 0.20) \times 10^{-11}$  cm<sup>3</sup> molecule<sup>-1</sup> s<sup>-1</sup> at 298 K.<sup>9</sup> No computational studies of the title

**Path1 P<sub>1</sub>** R→a1→P<sub>1</sub>  
**Path2 P<sub>1</sub>** R→a2→a3→a4→a5→a6→P<sub>1</sub>  
**Path3 P<sub>1</sub>** R→a2→a7→a6→P<sub>1</sub>  
**Path4 P<sub>1</sub>** R→a8→a9→b1→b2→a6→P<sub>1</sub>  
**Path5 P<sub>1</sub>** R→a8→a9→b3→b4→b5→P<sub>1</sub>  
**Path1 P<sub>4</sub>** R→b6→b7→b8→P<sub>4</sub>  
**Path6 P<sub>1</sub>** R→b6→b9→c1→c2→a5→a6→P<sub>1</sub>  
**Path7 P<sub>1</sub>** R→b6→c3→c2→a5→a6→P<sub>1</sub>  
**Path1 P<sub>2</sub>** R→c4→c5→c6→P<sub>2</sub>  
**Path1 P<sub>3</sub>** R→c4→c5→c6→c7→c8→P<sub>3</sub>  
**Path2 P<sub>2</sub>** R→c9→d1→d2→c6→P<sub>2</sub>  
**Path2 P<sub>3</sub>** R→c9→d1→d2→c6→c7→P<sub>3</sub>

**Figure 1.** Total reaction paths obtained at the QCISD(T)/6-311G(d,p)//UB3LYP/6-31G(d,p) level.

reaction have been reported. In this paper, we report the results of DFT calculations on the potential energy surface in order to elucidate the possible reaction paths.

**TABLE 1: Zero-Point, Total (au), and Relative Energies (kcal/mol) of Reactant, Products, and Isomers for the HCNO + NCO Reaction at the QCISD(T)/6-311G(d,p)//UB3LYP/6-31G(d,p) Level**

species	ZPE	QCISD(T)	QCISD(T) + ZPE
<b>a1</b>	0.036075	-335.942930	-41.3
<b>a2</b>	0.036073	-335.931261	-34.0
<b>a3</b>	0.036874	-335.947252	-43.5
<b>a4</b>	0.030138	-335.836133	22.0
<b>a5</b>	0.030705	-335.903877	-20.2
<b>a6</b>	0.030286	-335.906291	-21.9
<b>a7</b>	0.035670	-335.911511	-21.8
<b>a8</b>	0.035528	-335.893274	-10.5
<b>a9</b>	0.035431	-335.892707	-10.2
<b>b1</b>	0.035078	-335.891146	-9.4
<b>b2</b>	0.034098	-335.830173	28.2
<b>b3</b>	0.036598	-335.838516	24.5
<b>b4</b>	0.034444	-335.870632	3.0
<b>b5</b>	0.034229	-335.866858	5.2
<b>b6</b>	0.033154	-335.825993	30.2
<b>b7</b>	0.035355	-335.959746	-52.3
<b>b8</b>	0.029518	-335.975967	-66.1
<b>b9</b>	0.033942	-335.832808	26.5
<b>c1</b>	0.034115	-335.822795	32.9
<b>c2</b>	0.033276	-335.862699	7.3
<b>c3</b>	0.034228	-335.822547	33.1
<b>c4</b>	0.033448	-335.830651	27.5
<b>c5</b>	0.035453	-335.866497	6.3
<b>c6</b>	0.034620	-335.857070	11.7
<b>c7</b>	0.034631	-335.859838	9.9
<b>c8</b>	0.034886	-335.93648	-38.0
<b>c9</b>	0.035632	-335.822789	33.8
<b>d1</b>	0.033386	-335.821021	33.5
<b>d2</b>	0.033420	-335.838602	22.5
P <sub>1</sub> HCN + NO + CO	0.026030	-335.956369	-56.0
P <sub>2</sub> HCCO + NNO	0.030042	-335.884628	-8.5
P <sub>3</sub> CO <sub>2</sub> + HCN	0.030326	-335.959107	-55.1
P <sub>4</sub> HCO + N <sub>2</sub> + CO	<b>0.025095</b>	<b>-335.977452</b>	<b>-69.9</b>
R NCO + HCNO	0.028564	-335.869602	0.0

## Calculation Method

All calculations are carried out using the Gaussian 98 program.<sup>10</sup> The geometries of all the reactants, products, various

\* To whom correspondence should be addressed. E-mail: tianshiman@yahoo.com.cn.

<sup>†</sup> Shanxi Normal University.

<sup>‡</sup> Second Hospital of Jilin University.

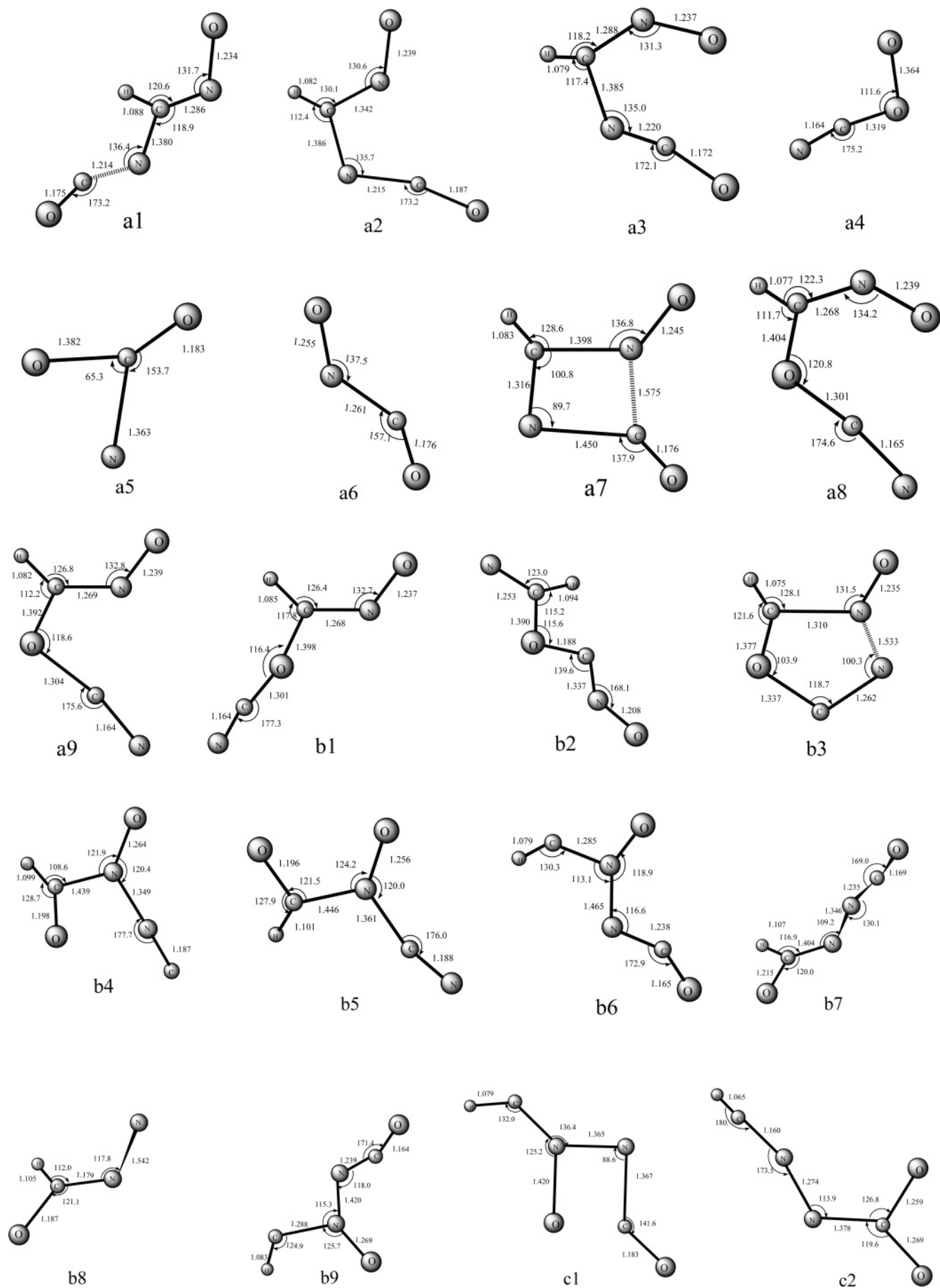
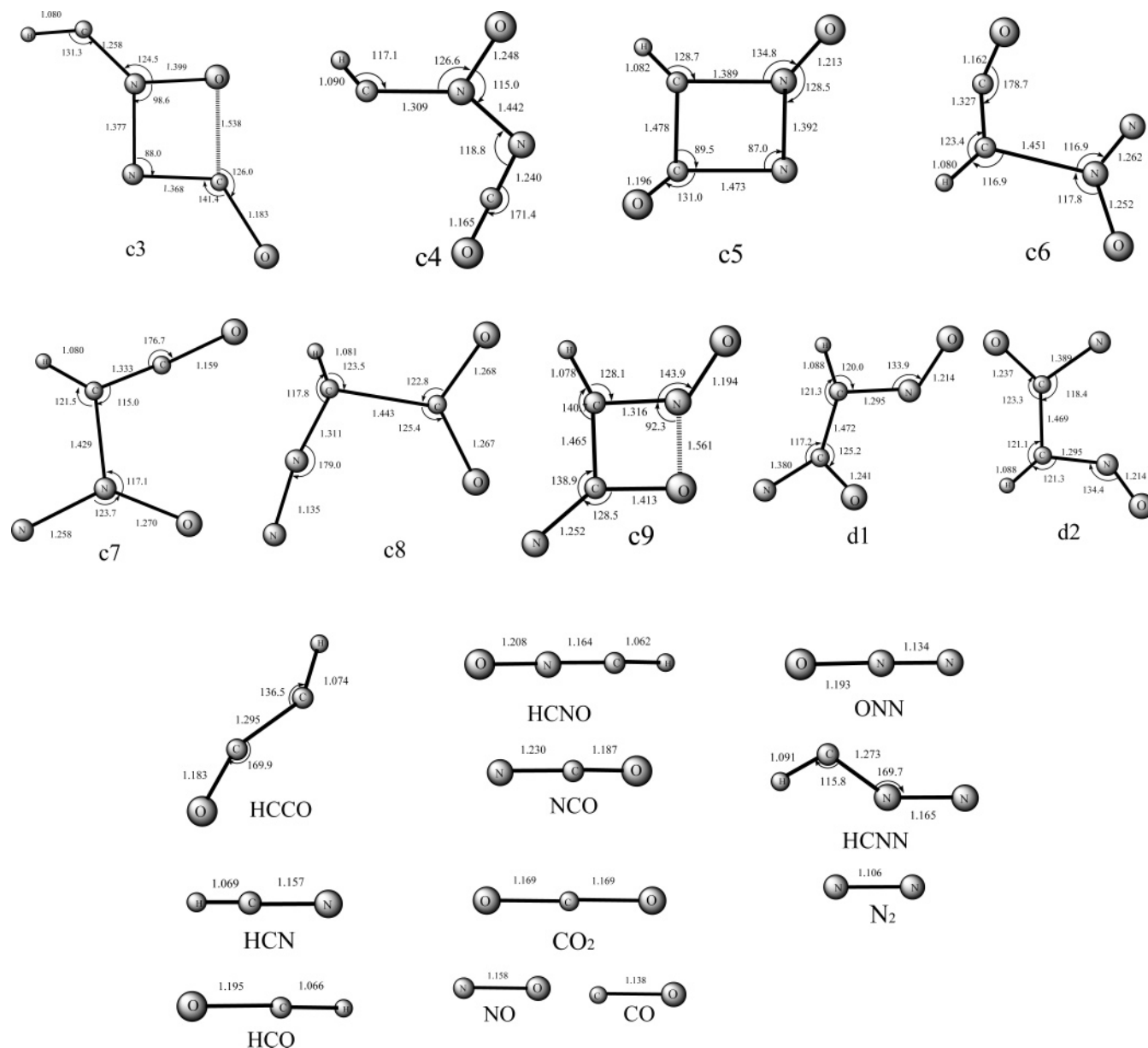


Figure 2. Part 1 of 2.



**Figure 2.** Part 2 of 2. The UB3LYP/6-31G(d,p)-optimized geometries of all isomers, the products, and the reactants. Bond distances are in angstroms and angles are in degrees.

intermediates, and transition states for the NCO + HCNO reaction are optimized using hybrid functional UB3LYP method with the 6-31G(d,p) basis set. Vibration frequencies are calculated at the UB3LYP/6-31G(d,p) level to check whether the obtained stationary points correspond to isomer or to first-order transition states. To confirm that the transition state connecting designated intermediates, we also perform intrinsic reaction coordinate (IRC) calculations at the UB3LYP/6-31G(d,p) level. In addition, single-point energies are calculated for the UB3LYP/6-31G(d,p) optimized geometries with the quadratic configuration interaction method with single and double excitation and perturbative corrections for triple excitations (QCISD(T)) with the 6-311G(d,p) basis set. Unless otherwise specified, the QCISD(T) single-point energies are used in the following discussion.

## Results and Discussion

**3.1. Initial Association Pathways.** Starting from the reactant **R** NCO + HCNO, we have obtained four energetically

accessible primary products (**P**<sub>1</sub>, HCN + NO + CO; **P**<sub>2</sub>, N<sub>2</sub>O + HCCO; **P**<sub>3</sub>, CO<sub>2</sub> + HCNN; and **P**<sub>4</sub>, N<sub>2</sub> + HCO + CO), and listed the reaction pathways in Figure 1. Figure 2 shows the optimized geometries of the reactants, products, and 24 intermediate isomers (denoted by the letters from a to d). The optimized structures of the transition states are shown in Figure 3. The reaction pathways related to the doublet [HC<sub>2</sub>N<sub>2</sub>O<sub>2</sub>] potential energy surface (PES) are schematically plotted in Figure 4. The energetic data of the reactants and products are listed in Table 1. The energy values of the transition states are listed in Table 2. All of the calculations are carried out at the QCISD(T)/6-311G(d,p)//UB3LYP/6-31G(d,p) level.

The attack of NCO at the HCNO molecule may have about 15 possible paths, i.e., end-N attack, end-O attack, middle-C attack, side N-C bonding attack, and side O-C bonding attack, etc. We tried all of the paths to associate NCO to the HCNO molecule, and found four feasible association paths. These paths are end-N attack to C, end-N attack to N, end-O attack to C, and middle-C attack to C. The end-N attack to C can form two

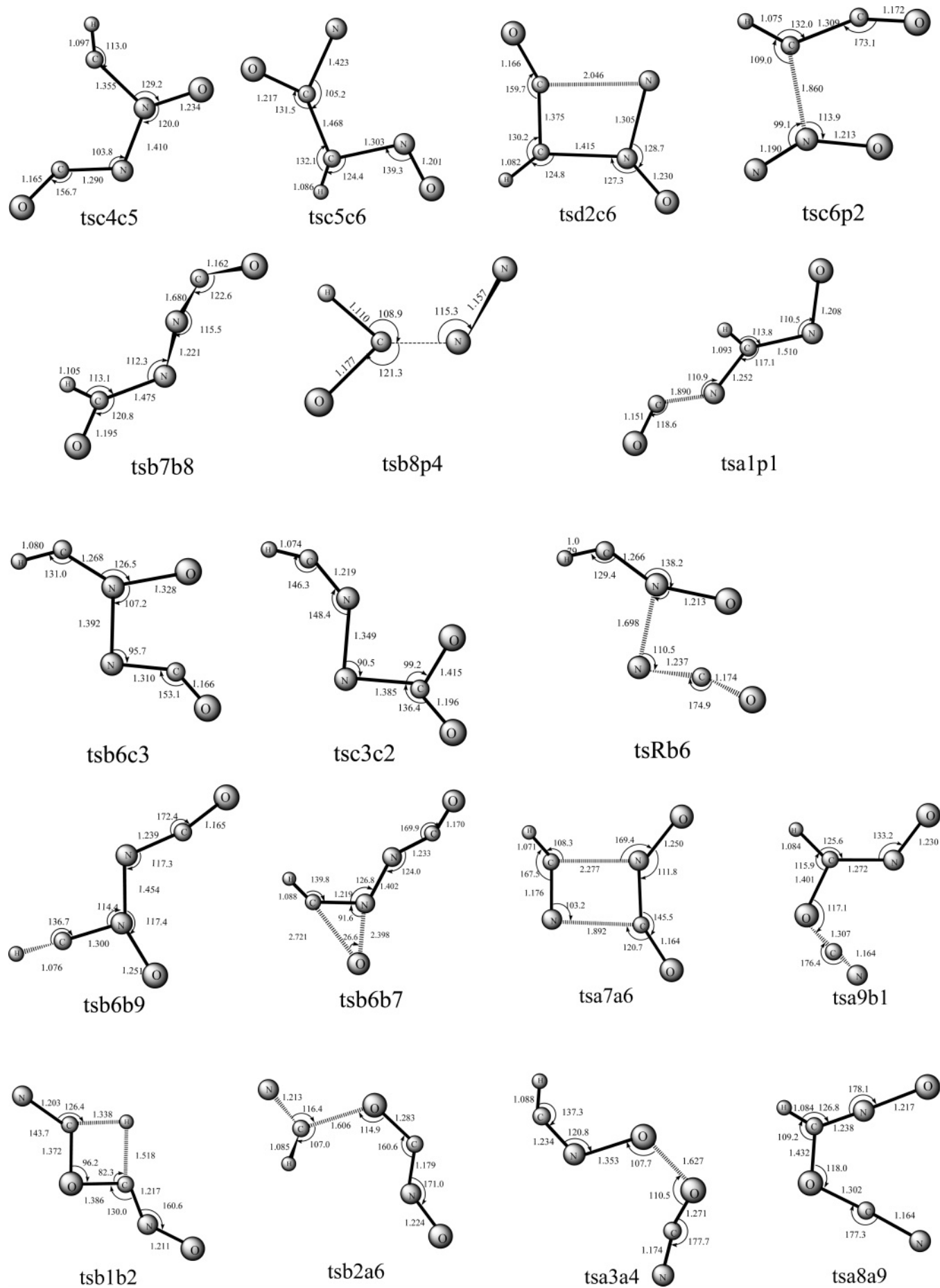
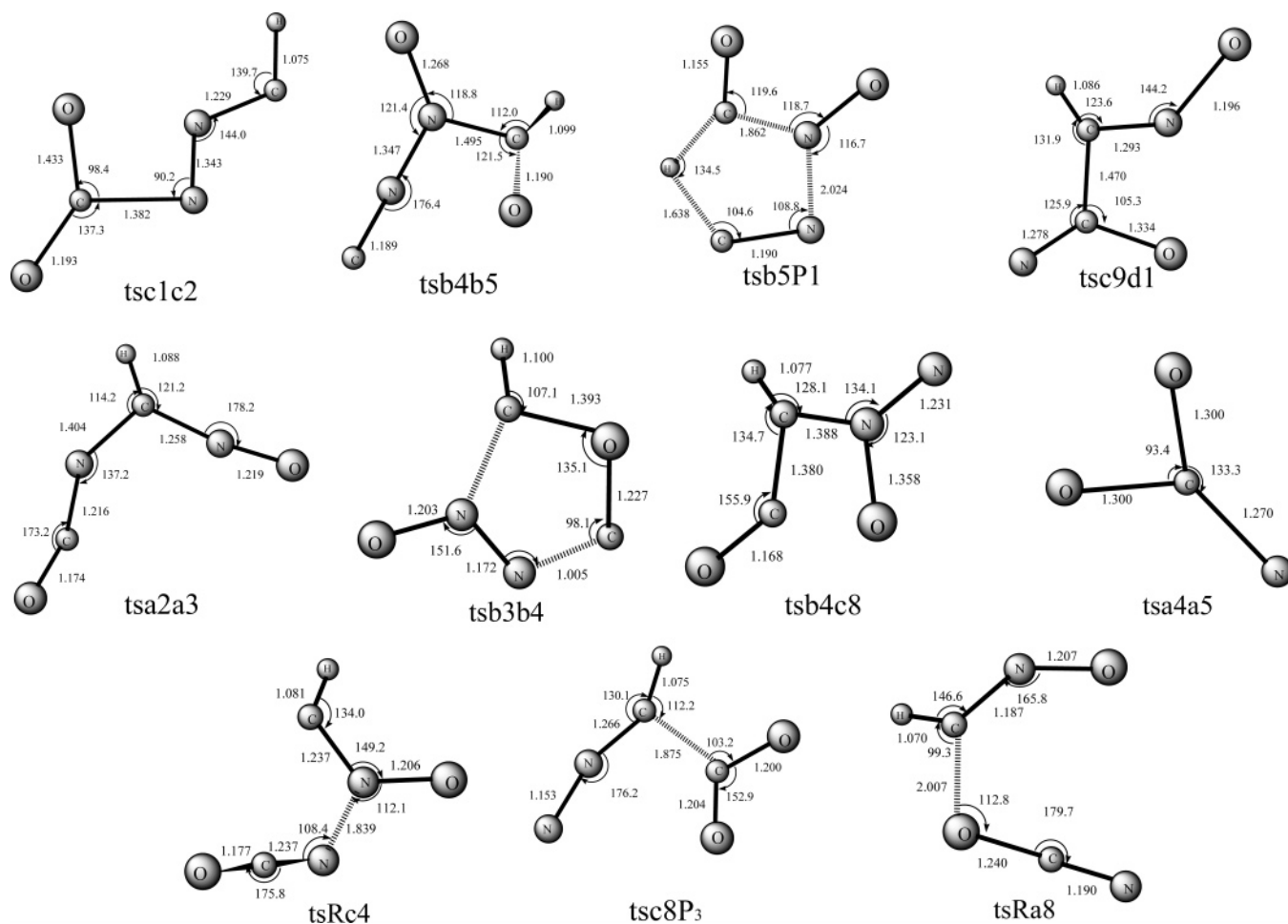


Figure 3. Part 1 of 2.



**Figure 3.** Part 2 of 2. The UB3LYP/6-31G(d,p)-optimized geometries of all transition states. Bond distances are in angstroms and angles are in degrees.

isomers **a2** and **a1**, which are directly linked with the reactant with two potential wells  $-34.0$  and  $-41.3$  kcal/mol, respectively. Other two isomers obtained from the end-N attack are isomers **b6** and **c4** located at  $30.2$  kcal/mol and  $27.5$  kcal/mol above the reactant, respectively. These two isomers are linked with the reactant by **TSRc4** for isomer **c4** and **TSRb6** for isomer **b6**. Clearly, these pathways involve substantial potential energy barriers. The C–C attack can form isomer **c9** after surmounting an energy barrier  $71.6$  kcal/mol of **TSRc9**. Isomer **a8** is resulted from the O-attack to the C atom and linked with the reactant by **tsRa8** lying at  $12.7$  kcal/mol above the reactant. Obviously, the end-N attack to the C atom should be more competitive than any other association ways because it is a barrierless association process. But these high-energy paths may be important in the high-temperature conditions.

**3.2. P<sub>1</sub>, P<sub>2</sub>, P<sub>3</sub>, and P<sub>4</sub>.** In this paper, 12 total reaction paths have been obtained and listed in Figure 1. The initially formed end-N attack isomer  $\text{HC}_2\text{N}_2\text{O}_2$  **a1** can dissociate to the product **P<sub>1</sub>** via two C–N single bonds ruptures. Isomer **a2** can further form a four-member ring **a7**, which can release the HCN fragment via the N–C bond rupture. The last ONCO fragment can further form the final NO and CO products through the N–C rupture. Another competitive reaction path is path 2 **P<sub>1</sub>**, which need to surmount **TSa3a4** lying  $69.5$  kcal/mol above the reactant. So this path cannot be expected feasible in low-temperature condition. It can be written as follows: isomer **a2** is converted to **a3** through the end-O atom vibration transition state, after which the O atom of the HCNO fragment is

abstracted, and the HCN fragment is emitted. The last  $\text{NCO}_2$  fragment isomerizes to the ONCO construction via an O-shift process from the C atom to the N atom (**TSa5a6**), and finally the products NO and CO molecules are emitted through the N–C bond rupture. Starting from **TSRa8** we can get two paths which need to undergo two high-energy transition states **TSb3b4** and **TSb1b2** lying at  $103.3$  and  $58.2$  kcal/mol above the reactant, respectively. Obviously it is difficult to surmount them in low-temperature condition. So from the dynamical view, these two paths are not important. Starting from **TSRb6** the reaction can proceed in three reaction paths and results in two species **P<sub>4</sub>** and **P<sub>1</sub>**. We simply describe the isomerization process starting from isomer **b6** in the following: (1) isomer **b6** undergoes a hydrogen shift followed by an N–C bond rupture, leading to product  $\text{CO} + \text{HCO} + \text{N}_2$ . We also located another high-energy transition state **TSb6b7** in this reaction path; (2) isomer **b6** undergo an end-H vibration followed by an O-shift process leading to **c2**, which looks like to rupture the N–C bond and emit the  $\text{CO}_2$  molecule. So we underwent many attempts to confirm a transition state to link isomer **c2** with the product  $\text{CO}_2 + \text{HCN}_2$ , but finally always ended up with **TSa2a5**, through which  $\text{HCN} + \text{NCO}_2$  can be produced. The conversion from  $\text{NCO}_2$  **a5** to ONCO **a6** needs to hurdle a high barrier  $94.6$  kcal/mol, so it is difficult to rupture further to  $\text{NO} + \text{CO}$ , at least in moderate temperature; (3) isomer **b6** can undergo an O-shift process followed by an O–N rupture, leading to isomer **c2**, which can proceed the same isomerization process as mentioned in path 1 and result in product  $\text{CO} + \text{HCO} + \text{N}_2$ .

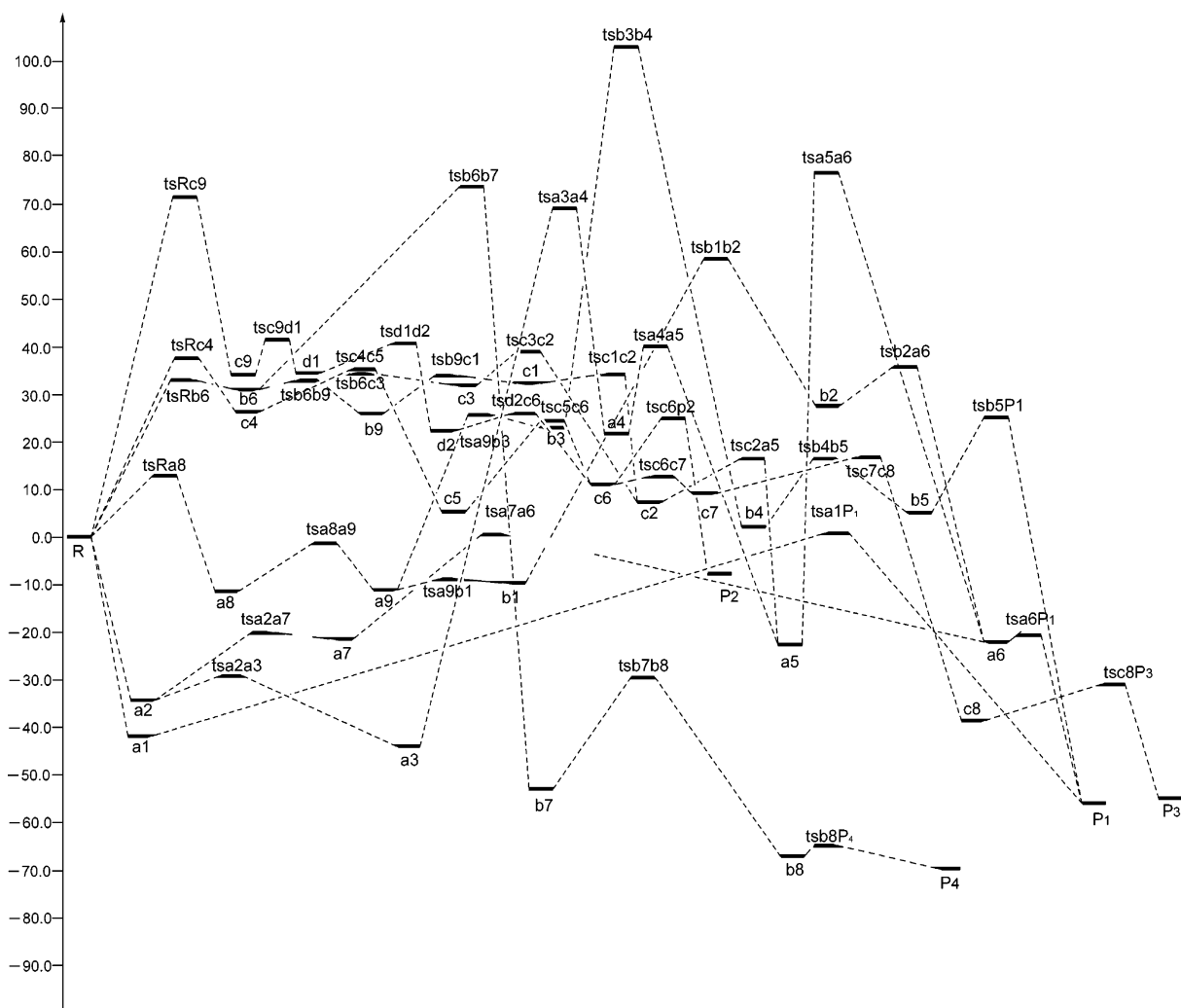


**Figure 4.** The potential energy surface of the relevant reaction pathways for the HCNO + NCO reaction at the QCISD(T)/6-311G(d,p)//UB3LYP/6-31G(d,p) level.

Isomer **c4** first formed the four-member ring **c5**, and then underwent two continual N–C bond ruptures leading to product **P2**. Alternatively it can also undergo an O-shift process followed by an N–C bond rupture to result in product **P3**. We also have found another path linking the reactant with **P2**: isomer **c9** can undergo an N–O rupture followed by a rotational isomerization and an N-shift process leading to the isomer **c6**, which can arrive at **P2** after an N–C bond rupture.

From the energy view, these four series of products are all feasible because all of them are located below the reactant on the potential energy surface, and the most stable product should be **P4**. Kinetically **P1** should have the largest branch ratio because its highest lying transition state lies at 1.4 kcal/mol above the reactant. This value is greatly lower than the barriers to the other product channels.

**3.3 Reaction Mechanism.** In section 3.2, we have obtained five important reaction channels which are most accessible for the NCO + HCNO reaction to produce four series of products. For these five reaction channels, the least competitive channel should be path 1 **P4** due to the high-energy transition state **TSb6b7**, which is 73.6 kcal/mol above the reactant and inaccessible in the combustion reactions. So though **P4** is the most stable product, we still have to regard it as the least competitive product in the combustion conditions. From Figure 4 we can find that isomer **c6** is the mutual isomer in both path 1 **P2** and path 1 **P3**. Furthermore, **TSb6b7** is located at 8 kcal/

mol above **TSb7b8**, which can result in **P3** finally over another transition state **TSb8P3**, so **P2** should be the second uncompetitive reaction product. There are two feasible reaction pathways path 3 **P1** and path 1 **P1** to produce **P1**. The relative energies of the determining transition states of these two reaction pathways are very similar; i.e., the barrier of **TSa7a6** in path 3 **P1** is 1.0 kcal/mol, and the barrier of **TSa1P1** in path 1 **P1** is 1.4 kcal/mol. But they are both much lower than the determination transition states of the other reaction pathways. Then we tentatively expect these two pathways may have comparable contributions to the NCO + HCNO reaction. Compared to **P3** and **P2**, **P1** should be more competitive not only thermodynamically but also kinetically.

As a result, reflected in the final product distributions, we predict that: (1) total four products **P1**, **P2**, **P3**, and **P4** should be detected in the experiments; (2) in both low and high-temperature conditions, the major product should be **P1**; (3) **P3** may be the second feasible product; (4) **P2** is the third competitive product; (5) **P4** is the least competitive product.

#### 4. Conclusions

A detailed doublet potential energy surface calculation of the HCNO + NCO reaction system has been carried out at the UB3LYP and QCISD(T) (single-point) levels. The main calculated results can be summarized as follows: (1) The most



**TABLE 2: Zero-Point (au), Total (au), and Relative Energies (kcal/mol) of Transition States for the Title Reaction at the QCISD(T)/6-311G(d,p)//UB3LYP/6-31G(d,p) Level**

species	ZPE	QCISD(T)	QCISD(T) + ZPE
TSc4c5	0.033187	-335.819038	34.6
TSc5c6	0.033796	-335.834228	25.5
TSc2a5	0.030743	-335.845822	16.3
TSd2c6	0.034217	-335.833858	26.0
TS6P2	0.031879	-335.832652	25.3
TSb7b8	0.031645	-335.919685	-29.5
TSa1P1	0.030337	-335.869185	1.4
TSb6c3	0.033649	-335.819606	34.5
TSc3c2	0.031341	-335.810866	38.6
TSRb6	0.032176	-335.820669	33.0
TSb6b9	0.032013	-335.820765	32.8
TSb6b7	0.029608	-335.753276	73.6
TSa7a6	0.030636	-335.870131	1.0
TSa9b1	0.034943	-335.889967	-8.8
TSb1b2	0.028752	-335.777017	58.2
TSb2a6	0.030791	-335.815362	35.4
TSa3a4	0.029981	-335.760290	69.5
TSa8a9	0.034305	-335.877661	-1.5
TSa9b3	0.035485	-335.835841	25.5
TSd1d2	0.032436	-335.822877	41.3
TSRc9	0.032049	-335.758955	71.6
TS9d1	0.032604	-335.807712	41.4
TSa2a7	0.035430	-335.908333	-20.0
TSa2a3	0.035312	-335.922666	-29.1
TSc6c7	0.034255	-335.854397	13.1
TSb9c1	0.033668	-335.821125	33.6
TSc1c2	0.031678	-335.817442	34.7
TSb4b5	0.033027	-335.848163	16.3
TSb3b4	0.029555	-335.705970	103.3
TSRa8	0.031399	-335.852182	12.7
TSb5P1	0.028096	-335.832657	22.9
TSRc4	0.031255	-335.813536	36.9
TSc8P3	0.032115	-335.922442	-30.9
TSb8P4	0.026839	-335.974075	-64.6
TSa6P1	0.027407	-335.900613	-20.2
TSa5a6	0.027156	-335.745467	77.0
TSa4a5	0.028032	-335.803925	40.9
TSc8P3	0.032115	-335.922400	-30.9
TSc7c8	0.034163	-335.8454824	17.2

feasible initial association way is the end-N attack of NCO at HCNO leading to  $\text{HC}_2\text{N}_2\text{O}_2$  **a1** via a barrierless process. Other

pathways involve high-energy barriers, and therefore do not play a major role at moderate temperatures; (2) Four total series of products can be obtained, **P<sub>1</sub>**, **P<sub>2</sub>**, **P<sub>3</sub>**, and **P<sub>4</sub>**. Among these products, **P<sub>1</sub>** is the most favorable product. **P<sub>3</sub>** is more feasible than **P<sub>2</sub>**, and **P<sub>4</sub>** is the least feasible product. These four products cannot further dissociate due to thermodynamical and kinetic factors; (3) The inner reaction mechanics for all of the feasible reactions paths are plotted in detail at the QCISD(T)/6-311g-(d,p)//UB3LYP/6-31G(d,p) level.

**Acknowledgment.** This work is supported by the National Science Foundation of China nos. 20471034 and 20673070.

## References and Notes

- (1) Miller, J. A.; Klippenstein, S. J.; Glarborg, P. *Combust. Flame* **2003**, *135*, 357.
- (2) Perry, R. A.; Siebers, D. L. *Nature* **1986**, *324*, 657.
- (3) Miller, J. A.; Bowman, C. T. *Int. J. Chem. Kinet.* **1991**, *23*, 289.
- (4) Siebers, D. L.; Caton, J. A. *Combust. Flame* **1990**, *79*, 31.
- (5) Chase, M. W. NIST-JANAF Thermochemical Tables. *J. Phys. Chem. Ref. Data*; 1998; 4th ed.
- (6) Schuurman, M. S.; Muir, S. R.; Allen, W. D.; Schaefer, H. F., III. *J. Chem. Phys.* **2004**, *120*, 11586.
- (7) Clifford, E. P.; Wenthold, P. G.; Lineberger, W. C.; Petersson, G. A.; Broadus, K. M.; Kass, S. R.; Kato, S.; Depuy, C. H.; Bierbaum, V. M.; Ellison G. B. *J. Phys. Chem. A* **1998**, *102*, 7100.
- (8) Osborn, D. L.; Mordaunt, D. H.; Choi, H.; Bise, R. T.; Neumark, D. M.; Rohlfing, C. M. *J. Chem. Phys.* **1997**, *106*, 10087.
- (9) Feng, W.; Herschberger, J. F. *J. Phys. Chem. A* [Online early access]. DOI: 10.1021/jp066036g.
- (10) Frisch, M. J.; Trucks, G. W.; Schlegel, H. B.; Scuseria, G. E.; Robb, M. A.; Cheeseman, J. R.; Zakrzewski, V. G.; Montgomery, J. A., Jr.; Stratmann, R. E.; Burant, J. C.; Dapprich, S.; Millam, J. M.; Daniels, A. J. *Phys. Chem. A* **2001**, *105* (43) 9910. Liu et al. D.; Kudin, K. N.; Strain, M. C.; Farkas, O.; Tomasi, J.; Barone, V.; Cossi, M.; Cammi, R.; Mennucci, B.; Pomelli, C.; Adamo, C.; Clifford, S.; Ochterski, J.; Petersson, G. A.; Ayala, P. Y.; Cui, Q.; Morokuma, K.; Malick, D. K.; Rabuck, A. D.; Raghavachari, K.; Foresman, J. B.; Cioslowski, J.; Ortiz, J. V.; Stefanov, B. B.; Liu, G.; Liashenko, A.; Piskorz, P.; Komaromi, I.; Gomperts, R.; Martin, R. L.; Fox, D. J.; Keith, T.; Al-Laham, M. A.; Peng, C. Y.; Nanayakkara, A.; Gonzalez, C.; Challacombe, M.; Gill, P. M. W.; Johnson, B.; Chen, W.; Wong, M. W.; Andres, J. L.; Gonzalez, C.; Head-Gordon, M.; Replogle, E. S.; Pople, J. A. *Gaussian98W*, Revision A.7; Gaussian, Inc.: Pittsburgh, PA, 1998.